Reconstruction

September 24, 2018

Contents

1 Reconstruction

While in the past Cherenkov detectors have been very successful in reconstructing various properties of the particles involved in a neutrino event, liquid scintillation detectors have long been thought as a source for calorimetric information only. However, in recent years it became obvious that the time information of the light in liquid scintillators can be used to access a wide range of information, similar or even superior to what a pure Cherenkov detector can deliver.

Basically, there are two complementary approaches to reconstruction in both detector types and consequently also in WBLS detectors. The first approach developed in MiniBooNE[1] and successfully applied in T2K[2] follows a likelihood ansatz to find the optimal track parameters and compare different hypotheses. In contrast to this, the three-dimensional topological reconstruction tries to picture the spatial distribution of the energy deposition within the detector without using a specific hypothesis. This technique has been developed for the LENA[3] detector and also been implemented for the JUNO detector [4]. These are liquid scintillator detectors, but the application to Cherenkov detectors is straight forward.

Both methods have been improved considerably over the last couple of years. For example fitQun, the reconstruction software used by T2K is now able to reconstruct up to 6 Cherenkov rings. This alone will increase the expected sensitivity for example for CP-violation in the LBNF beam significantly in comparison to previous studies like [5]. In addition, the topological reconstruction promises large volume liquid detectors the same capabilities as only highly segmented detectors used to have (with all the implications of that). This includes possibilities for particle identification at energies as low as a few MeV based on topological information. This ability will be further enhanced by the combination of the two light species, Cherenkov and scintillation light, as can be seen in [6], where Cherenkov-Scintillation separation is used to identify the two electrons of a $0\nu\beta\beta$-decay.

To give an overview on the state of the art in reconstruction, this section is divided into three subsections. The first subsection is dedicated to the likelihood approach and its latest results. The second subsection describes the topological reconstruction. And the third subsection is dedicated to applications of Cherenkov-light-Separation at low energies.

1.1 Likelyhood

This subsection summarizes the main features of the reconstruction method developed for the MiniBooNE detector[1]. In this method a likelihood function is evaluated for a particle (particles) of some type with initial kintmatic parameters to have produced the observed collection of PMT hits, charges and times, in an event. A key ingredient of the likelihood calculation is the predicted hit distribution which represents the average response of the detector for such a particle and therefore the likelihood is a function of the paricle's kinematic parameters. The optimal parameters would provide the best agreement between the predicted and observed hit distributions i.e. the likelihood function will be at a maximum.

Realistic model of detector response is required to develop a successful and efficient event reconstruction and identification algorithms. This requires both *in-situ* and *ex-situ* measurements of various optical properties of the water, PMTs and the

reflection of all surface inside the detector. Absorption, scattering, reflections and fluorescence processes can affect the reconstruction. In order to account for these effects in the reconstruction, these optical properties have to be obtained if unknown.

Single track is parametrized with 7 parameters: starting point (x_0, y_0, z_0), starting time t_0, direction θ_0, ϕ_0 with respect to the beam and kinetic energy E_0. We refer to this vector as $\mathbf{u}$. Track information is obtained by maximizing the likelihood that track with vector $\mathbf{u}$ will produce the observed PMT measurements. The likelihood for an event assuming all PMTs are independent is given by

$$L(\mathbf{q}, \mathbf{t}; \mathbf{u}) = \prod_{i}^{N_{unhit}} P_i(\text{unhit}; \mathbf{u}) \times \prod_{j}^{N_{hit}} P_j(\text{hit}; \mathbf{u}) f_q(q_j; \mathbf{u}) f_t(t_j; \mathbf{u}). \tag{1}$$

Here $P_i(\text{unhit}; \mathbf{u})$ is the probability PMT i is not hit given $\mathbf{u}$, $P_i(\text{hit}; \mathbf{u})$ is the probability PMT i is hit given $\mathbf{u}$, $f_q(q_j; \mathbf{u})$ is the probability density function for the measured charge q given $\mathbf{u}$ and predicted charge q_j, $f_t(t_j; \mathbf{u})$ is the probability density function for the measured time t given $\mathbf{u}$ evaluated time t_j. Product is carried over all PMTs. For convenience we can work with the negative logarithm of the likelihood which can be written as a sum of negative logarithms. We will use F_q and F_t to denote the charge and the time negative logarithm likelihoods respectively

$$-\log L(\mathbf{u}) \equiv F_q(\mathbf{u}) + F_t(\mathbf{u}), \tag{2}$$

$$F_t(\mathbf{u}) = -\sum_{i}^{N_{hit}} \log f_t(t_i; \mathbf{u}), \tag{3}$$

$$F_q(\mathbf{u}) = -\sum_{i}^{N_{unhit}} \log P_i(\text{unhit}; \mathbf{u}) - \sum_{i}^{N_{hit}} \log P_i(\text{hit}; \mathbf{u}) - \sum_{i}^{N_{hit}} \log f_q(q_i; \mathbf{u}). \tag{4}$$

From here on we will refer to F_q and F_t simply as the charge and the time likelihoods.

If the number of observed photoelectrons (PE), n_i, is known for a given PMT one can assume that $f_q(q_i; \mathbf{u})$ is fully specified regardless of detector properties. In addition, n_i can be assumed to be Poisson distributed with a mean value $\mu_i(\mathbf{u})$ (predicted charge) for which the notation μ_i will be used with implicit dependence on $\mathbf{u}$. As a result, the probability for a PMT to have no hit is

$$P_i(\text{unhit}; \mathbf{u}) \equiv \overline{P}_i(\mu_i) = e^{-\mu_i}. \tag{5}$$

Hence, the probability a PMT has recorded a hit is

$$P_i(\text{hit}; \mathbf{u}) \equiv P_i(\mu_i) = 1 - \overline{P}_i(\mu_i). \tag{6}$$

The next step is to separate the predicted charge into prompt and late predicted charge

$$\mu_i \equiv \mu_{prompt,i} + \mu_{late,i}. \tag{7}$$

The prompt predicted charge is a result of Čerenkov light, while the late predicted charge has contributions from direct Čerenkov light and indirect light. Sources of indirect light are reflections, scattering and fluorescence.

Time PDFs $f_t(t_i; \mathbf{u})$ depend on the first photon to fire the PMT. Dependence on $\mathbf{u}$ can be reduced by introducing corrected time

$$t_{cor,i} = t_i - t_0 - \frac{r_{mid,i}(E_0)}{c_n} - \frac{\Delta s_{mid}(E_0)}{c}, \tag{8}$$

where t_i is the measured PMT time, t_0 is the measured start time, $\Delta s_{mid}(E_0)$ is the distance from the track start point to the mean Čerenkov emission point, $r_{mid,i}(E_0)$ is the distance from the mean Čerenkov emission point to the PMT, c_n and c are the speeds of light in water and vacuum respectively. Due to the latency period PMT can register only one hit for a given track. Probabilities of no prompt PEs and no late PEs can be written as $P(\text{no prompt PEs}) = e^{-\mu_{prompt}}$ and $P(\text{no late PEs}) = e^{-\mu_{late}}$ respectively. The probability that a hit contains at least one prompt PE is

$$w_p = P(\text{prompt PE present}|hit) = \frac{1 - P(\text{no prompt PEs})}{1 - P(\text{no prompt PEs})P(\text{no late PEs})}. \tag{9}$$

This is the weight for the prompt primitive distribution $G_{ch}(t_c, E_0, \mu_{prompt})$, while the $w_l = 1 - w_p$ is the weight for the late primitive distribution $G_{late}(t_c, E_0, \mu_{late})$. Finally, the time PDF is obtained from

$$f_t(t; E_0, \mu_{prompt}, \mu_{late}) = w_p G_{ch}(t_c, E_0, \mu_{prompt}) + w_l G_{late}(t_c, E_0, \mu_{late}). \tag{10}$$

The primitives distribution are created by generating particles throughout the detector in special runs (e.g. only Čerenkov light and no scattering) and the response is parametrized.

1.2 3D topological reconstruction

In this subsection a reconstruction method is presented which aims to provide a 3D topological representation of the energy deposition of an event. The method has already been described in detail in [7]. Thus, here only a short description of the basic concepts is given.

Basic idea

The general idea of this method is to use the timing information of all registered signals for the construction of isochronal surfaces around each light sensor defined by the signal time. The overlap of these surfaces then indicates likely points of origin of the detected photons and thus can reflect the spatial distribution of the energy deposition of an event. The only assumptions made within this method are that a reference point on the topology is known reasonably well in space and time (the time of the energy deposition) and that all particles propagate through this point in approximately straight lines with the speed of light. The necessary reference point has to be provided by a prior analysis of the event. For the sake of simplicity we assume in the following that it is the primary vertex of the event. The isochrones can then be described by

$$c \cdot t_{signal} = |\overline{VX}| + n \cdot |\overline{XP}| \,, \tag{11}$$

where n is the effective refraction index for the scintillation light, $|\overline{VX}|$ is the distance between the vertex V of the event and the point of photon emission X, while $|\overline{XP}|$ is the distance between the point X and the PMT P.

These isochrones need to be smeared out using a time profile $F(t)$ given by the scintillator properties as well as the time resolution of the optical sensors used. This results in a probability density distribution for each signal. Furthermore, the position dependend light detection efficiencies of the PMT have to be taken into account as well as detector effects leading to different light emission in different regions (e.g. a buffer region). We combine these light distribution effects in the function $LD(\vec{x})$.

The full topological image of the event is then generated by adding up the individual probability density distribution $P_i(\vec{x})$:

$$P(\vec{x})_{total} = \sum_i P_i(\vec{x}) = \sum_i \left[\frac{F_i(t(\vec{x})) \cdot LD_i(\vec{x})}{\iiint F_i(t(\vec{x})) \cdot LD_i(\vec{x}) \cdot d\vec{x}} \right] . \tag{12}$$

Here, the index i indicates the individual signals. Thus the $F_i(t(\vec{x}))$ have to be evaluated with the individual signal times $t_{signal,i}$ and the position P_i of the PMT which detected the signal (see equation 13), while LD_i is an attribute of this PMT depending on its position, optics and sensitivity.

$$F_i(t(\vec{x})) = F_i\left((|\overline{VX}| + n \cdot |\overline{XP}|_i)/c \right) . \tag{13}$$

The result is a 3d map of the expected mean number of detected photons $\langle N_D(\vec{x}) \rangle$ coming from a given point. However, to get an impression of the energy deposition for a given event, the number of photons emitted from that point $\langle N_E(\vec{x}) \rangle$ is deciding. Therefore, every point of the 3d distribution has to be weighted by the inverse of the total signal detection efficiency $\eta(\vec{x})$ at that point:

$$\langle N_E(\vec{x}) \rangle = \frac{\langle N_D(\vec{x}) \rangle}{\eta(\vec{x})} = \frac{P(\vec{x})_{total}}{\sum_{PMT} LD_{PMT}(\vec{x})} \tag{14}$$

In principle, the reconstruction is completed at this stage. However, due to the large width of the time distribution of the individual signals, the picture may not seem very sharp. On the other hand, the large number of photons involved still generates a very good spatial resolution of the event topology. To extract this information, further algorithms are neccessary. For this purpose, standard algorithms developed originally for 2D image processing - like filtering, ridge-line finding, Sobel filter, etc. - can be adapted to accommodate 3D data.

Iteration procedure

In the method above all signals have been treated as completly independend of each other. However, this is not true because all of them belong to the same event and the resulting correlation can be described by the true event toplogy. This topology is of course unknown. However, if we dispose of a certain prior knowledge about that topology, we can express this as a 3D probability density distribution $PM(\vec{x})$. Instead of calculating our topological 3D-picture from the completely independent 3D probability density distributions $P(\vec{x})_i$, we can now calculate this topology under the condition that it has to match our knowledge $P(\vec{x}|PM(\vec{x}))_i$. In other words, if we already have a 3d representation of the event, which we call in this context

probability mask (PM), we can use this to reweight the 3D probability density distribution generated by every single photon prior to its normalisation: Thus the $P_i(\vec{x})$ in Equation 12 have to be substituted by

$$P_i(\vec{x}|PM(\vec{x})) = \frac{F_i(t(\vec{x})) \cdot LD_i(\vec{x}) \cdot PM(\vec{x})}{\iiint F_i(t(\vec{x})) \cdot LD_i(\vec{x}) \cdot PM(\vec{x}) \cdot dV} \tag{15}$$

A natural choice to generate a PM, is to use the reconstruction as described on the previous pages first without a PM. The result of this reconstruction then constitutes an unbiased representation of the event topology, which can then be used as the PM for a second iteration of the reconstruction. The result of this second reconstruction can again be fed back as a new PM into the reconstruction process. Thus an iterative procedure is created. The power of this iterative process can be seen in Fig. 1. Ultimately, this allows a close association of each signal photon with a certain volume of the event topology. This makes the energy deposition per unit length accessible as can bee seen in Fig. 1.

Results

So far this method has mainly been studied with the help of the LENA simulation. This simulation includes only an effective optical model and no Cherenkov light. Furthermore, it was assumed that every photon could be registered separatly. LENA has a coverage of 30% resulting in approximatly 250 detected photons per MeV. To reduce the computation time for the reconstruction an adaptive mesh was used. This allowed to establish a voxel size of 12.5 cm in the final iteration. More details about the simulation and the technical implementation of the topological reconstruction can be found in [7].

To proof the robustness and show the potential of this method a large sample of fully contained muons with energies between 1 and 10 GeV was used. An angular resolution between 1.4 at 1 GeV and 0.4 at 10 GeV could be achieved. In addition, the method has been implemented for the JUNO [4] detector. First results indicate a high potential for the separation of perfectly point-like events (electrons) from almost point-like events (positrons and gammas) at energies of a few MeV (compare [8]).

Application to Cherenov-light

Some modifications are needed for the application of this method to Cherenkov light. The most obvious one is the time profile $F(t)$, since the Cherenkov process emits the light instantaneously. Thus in most scenarios the timing profile of the photosensors will be the dominant factor, which can often be described by a Gaussian with the corresponding time resolution. However, chromatic dispersion of the Cherenkov light must be taken into account if sensors with very good time resolution (below 1 ns) are employed in detectors of the size of THEIA.

In addition the position dependent detection efficiencies also become direction dependent now, since the Cherenkov light is emitted only in a cone with respect to the particle direction. How to generate such direction dependent detection efficiencies is shown for example in [1]. However, in general they differ for different particles due to the different behaviour when passing through matter. To avoid this, we start instead with the basic method without any light distribution effect (detection

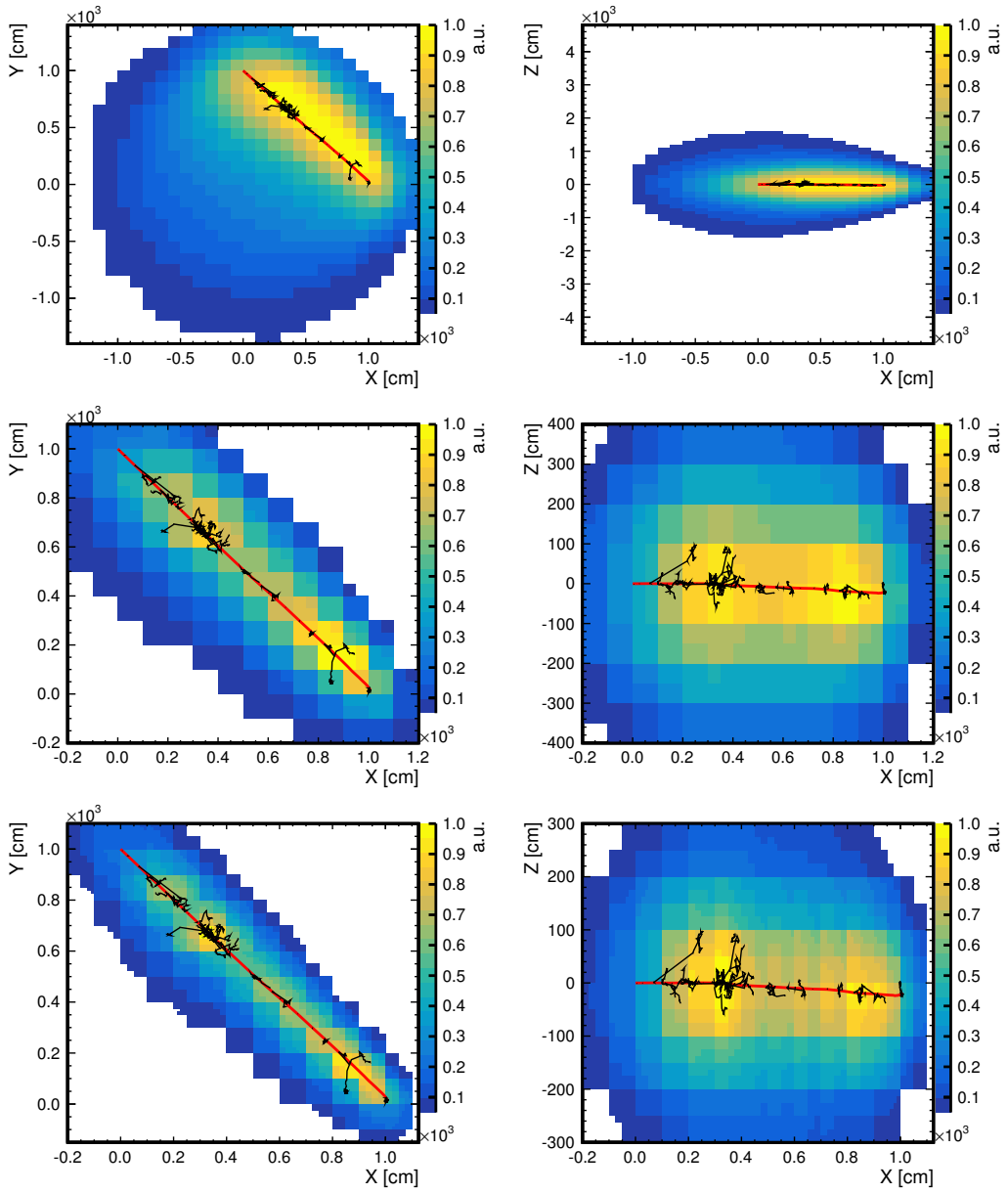

Figure 1: Reconstruction results after the iterations 0 (top), 8 (middle) and 21 (bottom) for a simulated muon with 3GeV initial kinetic energy in the cylindrical LENA detector projected along the symmetry axis (left) or a radial y-axis (right). The primary particle started at (0, 1000, 0)cm in the direction (1, −1, 0). Both the projected tracks of the primary particle (red) and of secondary particles (black) are shown. Note that both the axis scales and the sizes of the cells change due to the selection of a region of interest and the refinement of the reconstruction mesh. Moreover, the cell content is given in a.u. and rescaled such that the maximum content is 1. Some details on the actual reconstruction procedure are given in sec:Reconstruction.

efficiencies). Thanks to the good timing quality of the Cherenkov-light this already allows to define an accurate volume of interest. In principle, this toplogy can then

be used for the descion on the direction dependent detection efficiencies. However, this still has to be demonstrated.

1.3 Low energies reconstruction

by Andrey

References

[1] R.B. Patterson et al. The extended-track reconstruction for miniboone. *Nucl. Instrum. Meth. A*, 608(1):206–224, 2009.

[2] K. Abe et al. Measurements of neutrino oscillation in appearance and disappearance channels by the T2K experiment with 6.610^{20} protons on target. *Phys. Rev.*, D91(7):072010, 2015.

[3] Michael Wurm et al. The next-generation liquid-scintillator neutrino observatory LENA. *Astropart. Phys.*, 35:685–732, 2012.

[4] Fengpeng An et al. Neutrino Physics with JUNO. *J. Phys.*, G43(3):030401, 2016.

[5] J. Goon et al. The Long Baseline Neutrino Experiment (LBNE) Water Cherenkov Detector (WCD) Conceptual Design Report (CDR). 2012.

[6] Andrey Elagin, Henry Frisch, Brian Naranjo, Jonathan Ouellet, Lindley Winslow, and Taritree Wongjirad. Separating Double-Beta Decay Events from Solar Neutrino Interactions in a Kiloton-Scale Liquid Scintillator Detector By Fast Timing. *Nucl. Instrum. Meth.*, A849:102–111, 2017.

[7] Björn S. Wonsak, Caren I. Hagner, Dominikus A. Hellgartner, Kai Loo, Sebastian Lorenz, David J. Meyhoefer, Lothar Oberauer, Henning Rebber, Wladyslaw H. Trzaska, and Michael Wurm. Topological track reconstruction in unsegmented, large-volume liquid scintillator detectors. *JINST*, 13(07):P07005, 2018.

[8] B. Wonsak et al. 3d topological reconstruction in liquid scintillator detectors, 2018. Proceedings of 5th International Solar Neutrino Conference, Dresden, to be published.